Modelling of the GIA-induced surface gravity change over Fennoscandia

Per-Anders Olsson[1*], Jonas Ågren[1], Hans-Georg Scherneck[2]

June 15, 2012

[1]Geodetic Research Division, Lantmäteriet (Swedish mapping, cadastral and land registration authority), SE-801 82 Gävle, Sweden
[2]Onsala Space Observatory, Chalmers University of Technology, SE-439 92 Onsala, Sweden
[*]Corresponding author. Telephone: +46 771 63 63 63, Fax: +46 26 61 06 76, E-mail address: per-anders.olsson@lm.se

Abstract

This paper deals with the modelling of surface gravity change in Fennoscandia, induced by postglacial rebound or Glacial Isostatic Adjustment (GIA). The theoretical foundation is based on the theory introduced by [30, 34] for a spherical, non-rotating, laterally homogenous, viscoelastic, Maxwell Earth and the solution of the Sea Level Equation, originally introduced by [12], with time-dependent coastline geometry. The ice history is defined by the ice model ICE-5G. Rotational feedback is not included.

The sensitivity of predictions of present day gravity rates $\dot{g}$, with respect to a selection of assumptions and approximations, is investigated numerically. Six model variants are defined: i) linear relation between $\dot{g}$ and the vertical deformation rate $\dot{u}$, ii) direct attraction expressed in terms of internal and iii) external harmonic series expansions as well as by iv) analytical integration over rectangular prisms. For the most rigorous treatment of the direct attraction, the effect of simplified modelling of the sea level is also investigated. These modelling approximations of the sea level change include v) fixed shorelines and vi) eustatic sea level change. Predictions of $\dot{g}$ for the model variants are plotted, compared and discussed.

The most rigorous model iv) and the linear model i) differ less than 0.03 μGal yr^{-1} over land and close to, or over, the ocean the difference reaches maximally ~ 0.5 μGal yr^{-1}. Due to truncation at degree 180, the high frequent nature of the direct attraction is not properly described by model ii) and iii). The two simplified sea level modelling approximations v) and vi) induce differences, compared to the most rigorous model exceeding 0.2 μGal yr^{-1} over land, i.e. about one order of magnitude worse than the linear model.

Keywords: Glacial isostatic adjustment, postglacial rebound, gravity change, Fennoscandia

1   Introduction

The postglacial land uplift in Fennoscandia in Northern Europe is a well known phenomenon and a result of the still ongoing Glacial Isostatic Adjustment (GIA) after the Pleistocene glaciation. The region has a long history of observations of the GIA induced vertical displacement of the crust in terms of i) relative sea level observations (see e.g. [8, 9, 17]), ii) repeated levellings (e.g. [2, 8]) and iii) continuous GNSS observations (e.g. [35]). Various land uplift models for this region have been published, e.g. [8, 18] (empirical), [17, 24] (geophysical) and [2, 14] (combination of empirical and geophysical). The empirical models have played an important role for reduction of geodetic observations to a certain epoch while the aim of geophysical modelling often has been to study and constrain geophysical Earth parameters, e.g. the mantle viscosity profile.

In addition to vertical and horizontal displacement of the crust the GIA process also induces changes in the gravitational field. An early effort to measure the GIA induced gravity change in Scandinavia was the establishment of the Fennoscandian land uplift gravity lines in 1966. They consist of four east-west profiles across the Fennoscandian postglacial rebound area, along which repeated relative gravity measurements have been performed between 1966 and 2003 [21, 22]. This work was coordinated by the Nordic Geodetic Commission (NKG), which is an organized collaboration between geodesists in the Nordic countries.

One important purpose with these observations was to determine the relation between land uplift and gravity change and thereby make conclusions on the underlying geodynamic processes. Based on these relative gravity observations, precise levelling, tide gauge data and their respective observational accuracies, [10] found the ratio between the rate of change of gravity $\dot{g}$ and the land uplift rate $\dot{u}$ to be -0.204 ± 0.058 μGal mm^{-1}. Recently [23] examined absolute gravity and GPS time series in North America and found a $\dot{g}/\dot{u}$ ratio of -0.17 ± 0.01 μGal mm^{-1}. Several papers investigate the ratio theoretically. [42] approximated the viscous part of the ratio by the linear relationship -0.154 μGal mm^{-1} and motivated it as to being satisfactory when only the M0 mode of a homogeneous earth is considered. [6] investigate the spectral behavior of the ratio for a self-gravitating, spherical, elastic Earth and [11] showed that the gravity-uplift ratio is almost independent of the viscosity structure, and compressible or incompressible mantles.

During the last decade the relative measurements in the Fennoscandian land uplift gravity lines have been succeeded by a comprehensive cooperation between institutions in and around the Fennoscandian area. Also this work is coordinated within the Nordic Geodetic Commission (working group of Geodynamics). Using FG5 absolute gravimeters the absolute gravity change is observed with one or a few years interval at a number of stations. One important long term goal of this Nordic Absolute Gravity Project is to acheive a model of the present-day rate of change of gravity, accurate enough for reduction of geodetic observations to a certain epoch.

A recent and comprehensive review of GIA-related modelling and data in

Fennoscandia is given by [40].

The accuracy of the observed gravity change and the three dimensional deformation of the crust successively increases. This, at the same time, demand and enable a more accurate modelling of the postglacial rebound in general and of the gravity change in particular. In light of the increased activity concerning gravity observations and coming updates of national gravity reference systems in some of the Nordic countries, Nordic geodesists are discussing how the gravity change should be modelled. How well does a constant linear relation between $\dot{g}$ and $\dot{u}$ represent local ratios of $\dot{g}/\dot{u}$ in the region? Does a more rigorous GIA-modelling of $\dot{g}$ differ substantially from the linear model? How sensitive are the $\dot{g}$ predictions to different ways of modelling the relative sea level variations?

The purpose of this paper is to study, show and discuss how predictions of present day surface gravity change in Fennoscandia is affected by assumptions and approximations in the GIA-modelling, with emphasis on the direct attraction and sea level variations. Assuming a certain Base Model (BM), six model variants are defined and $\dot{g}$-predictions from all model variants are plotted and compared. The model variants differ in terms of how the direct attraction is treated (internal- or external harmonic series expansions or integration over rectangular prisms) and how the sea level variations are modelled (with and without migrating shorelines and eustatic).

In the next section the GIA-modelling method (the Base Model) is described, followed in Section 3 by a description of the six model variants. Numerical results, i.e. $\dot{g}$ predictions from the model variants, are presented in Section 4 and discussed in Section 5. Finally some conclusions on the results as well as an outlook on future work is given.

2 Method

Our GIA-model is based on the theory described by e.g. [30, 5, 34, 31, 43, 44, 45], that is, the normal mode method for a spherical, non-rotating, laterally homogenous, viscoelastic Earth as an extension of the work of [19, 20] and [13] who considered an elastic body only. The sea level variations are found by solving the Sea Level Equation, originally introduced by [12]. Time dependent coastlines, first adressed by [15], are here treated according to the Generalized Sea Level Equation as described by [25] and [16]. The most rigorous treatment of the direct attraction of present-day sea level variations include integration over rectangular prisms for nearby water masses. Earth's rotational feedback (with a node line right through Fennoscandia), first adressed by [4], is not included. In this section we give a short presentation of the method and the most important formulas used.

We aim to predict and evaluate the present vertical displacement rate $\dot{u}$ and rate of change of gravity $\dot{g}$. Numerically, we compute them as the average change during the last 100 years

$$\dot{u} \quad \approx \quad \frac{u(t_p) - u(t_{p-100})}{100} \tag{1}$$

<div align="center">3</div>

$$\dot{g} \approx \frac{\Delta g(t_p) - \Delta g(t_{p-100})}{100} \tag{2}$$

where t_p is present time and t_{p-100} is 100 years before present. Based on the assumption of isostatic equilibrium at Latest Glacial Maximum (LGM), the surface vertical displacement u and gravity change Δg, since the assumed isostatic equilibrium at LGM, is found by convolving appropriate Green's functions G in time and space, with a function L of the temporal and spacial evolution of the loading of the Earth [34] (with notation from [36]),

$$\begin{bmatrix} u \\ \Delta g \end{bmatrix} (\omega, t) = \int_{-\infty}^{t} dt' \int_{\Omega} \begin{bmatrix} G_u \\ G_g \end{bmatrix} (\theta, t - t') L(\omega', t') d\Omega, \tag{3}$$

where ω and ω' are the spherical coordinates of the point of observation and the loading point respectively, t and t' are the times of observation and loading respectively and Ω denotes the area of the whole sphere (Earth). Equation (3) is solved by means of numerical integration (midpoint method) over a 0.1×0.1 degree grid and turns into

$$\begin{bmatrix} u \\ \Delta g \end{bmatrix} (\omega, t) \approx \sum_{t'=t_{LGM}}^{t} \sum_{\Omega} \begin{bmatrix} G_u \\ G_g \end{bmatrix} (\theta, t - t') L(\omega', t') \Delta \Omega \Delta t \tag{4}$$

where t_{LGM} is 21 kyrs before present, subsequent timesteps 1 kyr and the spatial resolution 0.703×0.703 degrees for the ice load and 1×1 degree for the ocean load (see below). The load in each cell is concentrated to a point in the middle of the cell. Green's function for vertical displacement G_u and gravity G_g are respectively [20]

$$G_u(\theta, t) = \frac{1}{g_E} \frac{G}{a} \sum_{n=0}^{\infty} h'_n(t) P_n(\cos \theta) \tag{5}$$

$$G_g(\theta, t) = \frac{G}{a^2} \sum_{n=0}^{\infty} \left[-n - 2h'_n(t) + (n+1)k'_n(t) \right] P_n(\cos \theta) \tag{6}$$

where the positive direction for the vertical displacement is along the radial vector (up) and for gravity in the opposite direction (down). G is the gravitational constant, a is the radius of the spherical Earth, g_E is the normal gravity value, P_n are Legendre polynomials of degree n and θ is the spherical distance between the point of observation ω and the loading point ω'. $h'_n(t)$ and $k'_n(t)$ are time dependent, viscoelastic load Love numbers [30], one for each spherical harmonic degree. The viscoelastic load Love numbers are constructed as a combination of elastic (h^e_n, k^e_n) and viscous (h^v_n, k^v_n) load Love numbers and corresponding relaxation times τ such that

$$\begin{bmatrix} k'_n \\ h'_n \end{bmatrix} (t) = \begin{bmatrix} k^e_n \\ h^e_n \end{bmatrix} \delta(t) + \sum_{i=1}^{M} H(t) \begin{bmatrix} k^v_{ni} \\ h^v_{ni} \end{bmatrix} e^{s_{ni} t} \tag{7}$$

4

where M is the number of viscous modes, δ is the delta impulse function, H is a Heaviside step function and s is the negative of the inverse relaxation time, $s = -\tau^{-1}$. We have used the software TABOO [38, 37] to compute $h_n^e, k_n^e, h_n^v, k_n^v$ and τ for harmonic degrees 2-180 with the following incompressible Earth model:

- Averaged version of PREM [7] expressly built for the software TABOO [37] (Number of viscous layers = 2, Code = 0) with

- 90 km thick elastic lithosphere,

- upper mantle (above 670 km) viscosity $0.52 \cdot 10^{21}$ Pa s,

- lower mantle (below 670 km) viscosity $2.8 \cdot 10^{21}$ Pa s,

where the upper and lower mantle viscosities are the arithmetic means of the viscosity model VM2 [33] for the corresponding depth intervals. VM2 was introduced by [32] together with the ice model ICE-5G (see below).

In equations (3) and (4), the Green's functions are convolved over a loading function L. The load is composed of two components, both governed by the accumulation and ablation of ice; one is the ice loading itself and the other is the loading from the meltwater unevenly distributed over the oceans.

$$L(\omega, t) = L_{ice}(\omega, t) + L_{ocean}(\omega, t) \tag{8}$$

We have applied the ice history from the ice model ICE-5G [32] as

included in the software SELEN version 2.7 [36] with

- discrete point loads (0.703×0.703 degree grid),

- discrete time steps (1000 yrs) from 21 kyrs before present till present and

- isostatic equilibrium assumed at model start (latest glacial maximum).

When it comes to the ocean load history we have solved the Sea Level Equation (SLE) without rotational feedback, originally introduced by [12] (using the notation from [36])

$$S = \frac{\rho_i}{g_E} G_s \otimes_i I + \frac{\rho_o}{g_E} G_s \otimes_o S + S_E - \frac{\rho_i}{g_E} \overline{G_s \otimes_i I} - \frac{\rho_o}{g_E} \overline{G_s \otimes_o S} \tag{9}$$

where S is the relative sea level change since the model start (isostatic equilibrium at LGM), ρ_i and ρ_o are the densities of the ice and the water respectively, $\otimes$ denotes convolution in time and space (corresponding to (3)) over the load I and S (change in ice height and relative sea level respectively). $G_s = G_\phi/g - G_u$ is Green's function for the sea level, where

$$G_\phi = \frac{G}{a} \sum_{n=0}^{\infty} (1 + k_n') P_n(\cos \theta) \tag{10}$$

5

is the Green's function for perturbation of the gravitational potential. S_E is the "eustatic" sea level change, which for each time step is defined by

$$S_E = -\frac{m_i}{\rho_o A_o} \tag{11}$$

where m_i is the change in ice mass and A_o is the total area of the ocean. The overline over the last two terms in (9) denotes the spatial average over the ice and oceans respectively, and together the three last terms represent a change of the sea surface (geoid) to a new geopotential level.

The Sea Level Equation (9) as provided by [12] is based on the assumption that the coastline is not changing with the sea level. To model the variation of the coastlines, we have adopt the generalized version of SLE introduced by [25] and [16]

$$S_{ol}(t') = S(t')C(t')\beta(t') - T(t_0)[C(t')\beta(t') - C(t_0)\beta(t_0)] \tag{12}$$

where S_{ol} is the "true" change in ocean load (ocean height), defined as the change in the vertical distance between the physical sea *surface* and the solid surface, from time t_0 to time t' at any point in the ocean. S is the relative sea *level* change in (9), valid on the entire Earth (land and sea) and based on the assumption on non-varying (vertical) coastlines. T is the topography, i.e. the vertical distance from the solid surface to the sea level (geoid). The ocean function C is defined as

$$C = \left\{ \begin{array}{ll} 1 & \text{if } T < 0 \text{ (ocean)} \\ 0 & \text{if } T \geq 0 \text{ (land)} \end{array} \right. \tag{13}$$

and

$$\beta = \left\{ \begin{array}{ll} 1 & \text{where there is no grounded ice} \\ 0 & \text{where there is grounded ice.} \end{array} \right. \tag{14}$$

The height model ETOPO1 [27] was used as a first approximation of the topography $T(t_0)$ at latest glacial maximum (21 kyrs before present). After solving SLE a new approximation of $T(t_0)$ (and $T(t')$ at all consecutive time steps) is found from

$$T(t') = T(t_p) + S(t_p) - S(t') \tag{15}$$

where S is the relative sea level change since t_0, and t_p is present time. The ocean function $C(t')$ is then determined based on the new estimation of $T(t')$. After each such iteration of the full glacial cycle, the value of S for all grid cells is compared with the corresponding value from the previous iteration. The largest difference compared to the previous iteration was 1072 (compared to 0), 124, 36, 11 and 3 meters respectively for 5 iterations of the full glacial cycle.

The model described in this section will henceforth serve as our Base Model. Variants of this model are widely used. The purpose of the rest of this paper is to show how some simplifications and/or extensions of this base model will affect the predicted $\dot{g}$ in Fennoscandia.

3 Model variants

In this section we introduce a few variants of the Base Model (BM) described in the previous section. The variants are presented here with a name an abbreviation by wich they will be referred to in the following. Table 1 gives an overview and summary of the model variants.

3.1 Base Model (BM), internal series

This is the model described in section 2. In it, Green's function for gravity is given by

$$G_g = \frac{G}{a^2} \sum_{n=2}^{180} \left[-n - 2h'_n + (n+1)k'_n \right] P_n(\cos\theta). \tag{16}$$

The first term (corresponding to the direct attraction from the loading masses) is here expressed in terms of an internal series, that is, it is assumed that the point of observation is located below the attracting masses. This is how Green's function of gravity is presented in many classical papers, e.g. [20, 13, 30] (although with the opposite sign, since in these papers the direction of gravity is choosen positive upwards while we have choosen gravity to be positive downwards). Note that if the attracting masses are located at a lower altitude than the point of observation, which is the case for the effect of sea level variations on a gravimeter located on land, then the direct attraction in an internal series will contribute with the wrong sign, cf. Section 3.2. For practical reasons the summation is truncated at $n_{max} = 180$.

3.2 External Series (ES)

If the attracting masses are located below the point of observation then the first term in Green's function for gravity should be expressed in terms of an external series

$$G_g = \frac{G}{a^2} \sum_{n=2}^{180} \left[(n+1) - 2h'_n + (n+1)k'_n \right] P_n(\cos\theta). \tag{17}$$

Except for the first term in equation (17) the ES-model is the same model as (BM).

3.3 Linear Relation to $\dot{u}$ (LR)

Predictions of $\dot{g}$ is often approximated with a linear relation to $\dot{u}$ (e.g. in [42, 10]), such that

$$\dot{g} = C \cdot \dot{u}. \tag{18}$$

We want to compare this approximation with more rigorous modelling of $\dot{g}$. Our LR-model is based on $\dot{u}$ modelled with equations (1), (4) and (5) and $C = -0.154\ \mu\text{Gal mm}^{-1}$ from [42].

7

3.4 Full Solution (FS)

To fully catch the high frequent nature of the direct attraction and include the effect of the height of the point of observation the first term in equation (6) is here replaced by a more rigorous treatment. For loading grid cells close to the point of observation the direct attraction is solved by analytical integration over rectangular prisms. Also for grid cells further away the direct attraction is solved analytically, but the load is here represented by point loads (see Figure 1).
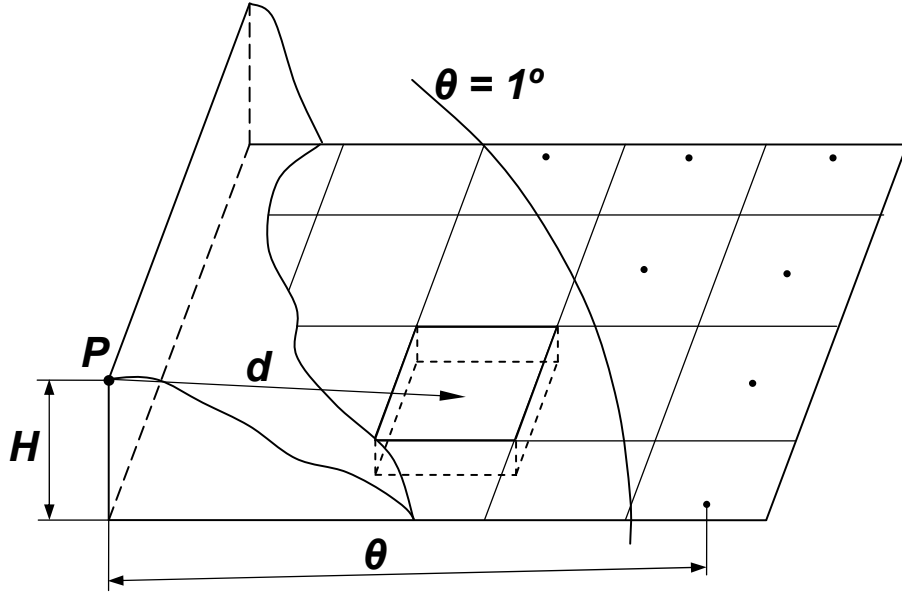
Figure 1: Geometry for how the direct attraction is treated in the Full Solution.

For $\theta < 1°$ the first term in Green's function for gravity is replaced by analytical integration over rectangular prisms. Figure 2 shows one loading grid cell i represented by a rectangular prism. The coordinates for i are given in a Cartesian coordinate system with origin in the point of observation P. The z-axis coincides with the radial direction of the spherical earth at P. The gravitational potential $\phi^i(P)$ from i at P is

$$\phi^i(P) = G\rho^i \int\limits_{x_{1i}}^{x_{2i}} \int\limits_{y_{1i}}^{y_{2i}} \int\limits_{z_{1i}}^{z_{2i}} \frac{1}{d} dx dy dz \tag{19}$$

where ρ_i is the density of the loading mass, $d = \sqrt{x^2 + y^2 + z^2}$, $x_i = a(\Phi_i - \Phi_P)$ and $y_i = a\cos\Phi_P(\Lambda_i - \Lambda_P)$; Φ is the latitude and Λ is the longitude of the point in question. For present day Fennoscandia the only surface mass variations

8

taking place are related to sea level variations. In this case z_2 is the height of the sea surface above P (corresponds do negative H in Figure 1). $z_2 - z_1$ corresponds to the relative sea level change and $\rho^i = \rho_{water} = 1030$ kg m^{-3}. Now the radial composant of the gravitational vector between P and i is

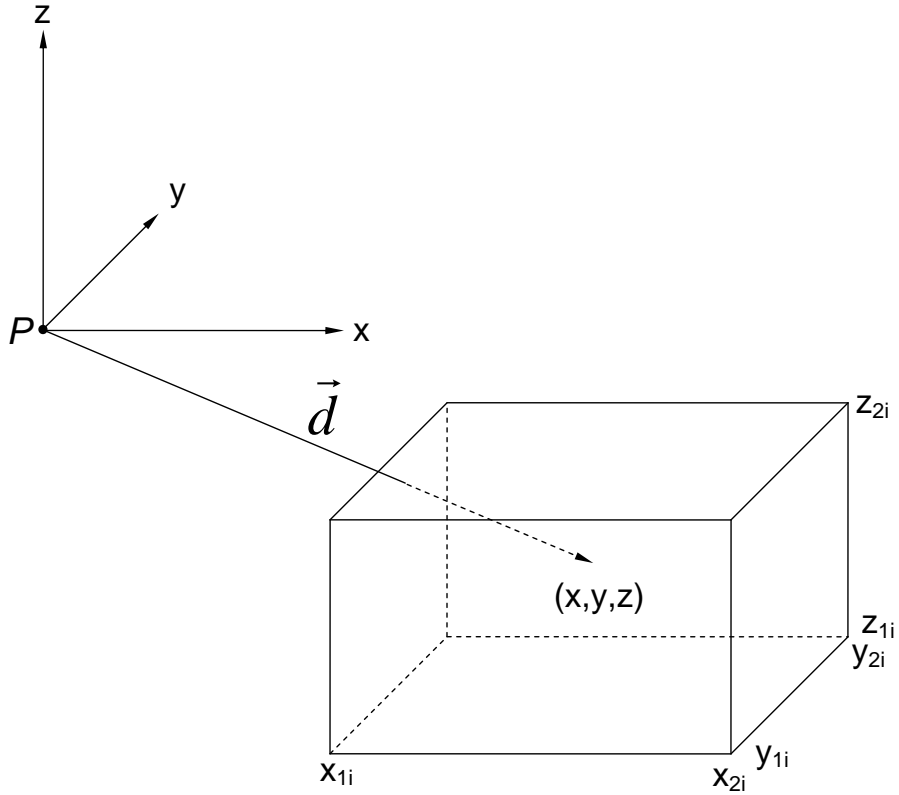$$g_N^i(P) = -\frac{\partial \phi^i}{\partial z_P}. \tag{20}$$

Figure 2: Notation for the analytical integration over rectangular prisms.

Eqs (19) and (20) can be combined and analytically derived as (see e.g. [1, 26])

$$g_N^i(P) = G\rho_w \left\| \left| \left| x\log(y+d) + y\log(x+d) - z\arctan\left(\frac{xy}{zd}\right) \right|_{x_{1i}}^{x_{2i}} \right|_{y_{1i}}^{y_{2i}} \right|_{z_{1i}}^{z_{2i}}. \tag{21}$$

Since the horizontal distance between the point of observation and the loading mass is always less than one degree, no correction for the curvature of the earth has been applied.

For $\theta > 1$ the loading masses are treated as point loads. Also in this case the direct attraction is computed analytically. The Newtonian attraction from a unit point load is now expressed as a function of the spherical distance θ and the difference in height H between the point of observation and the loading point (Figure 1) and is now included in Green's function for gravity such that

$$G_g = \frac{G}{a^2} \left(t^2 \frac{1 - t\cos\theta}{(1 - 2t\cos\theta + t^2)^{3/2}} + \sum_{n=2}^{180} \left[-2h'_n + (n+1)k'_n \right] P_n(\cos\theta) \right). \quad (22)$$

where $t = a/(a+H)$ (c.f. [29]). Eq. (22) accounts for the difference in height between the point of observation and the loading point as well as for the curvature of the earth.

3.5 Fixed Coastline geomentry (FC)

This model is the same as FS but the Sea Level Equation is solved once (i.e. no iterations of the full glacial cycle). This means that present coastlines geometry and seafloor topography (taken into account when ice ablate from the seafloor) are used throughout the computations.

3.6 Eustatic Sea Level (ESL)

This model is the same as FC but the sea level change is modelled by equation (11) instead of (9) and (12).

Table 1: Summary of the model variants described in Section 3. GSLE stands for Generalized Sea Level Equation (see Section 2, equation (12)).

Model		Direct attraction	Sea Level Model
Base Model	BM	Internal series	GSLE
External series	ES	External series	GSLE
Linear relation	LR	No	GSLE
Full solution	FS	Analytical	GSLE
Fixed coastlines	FC	Analytical	Fixed coastlines
Eustatic sea level	ESL	Analytical	Eustatic variation

4 Numerical results

In this section predictions of present-day $\dot{g}$ are plotted for each model variant described in Section 3. Over land the points of observation are located on the solid surface. Over sea this corresponds to the effect experienced by a gravimeter located on an infinitely small island or platform grounded on the sea floor; however it would not be valid on the sea surface itself. This is because the sea surface does not experience the vertical movement of the solid crust modelled by the h'-term in equation (6).

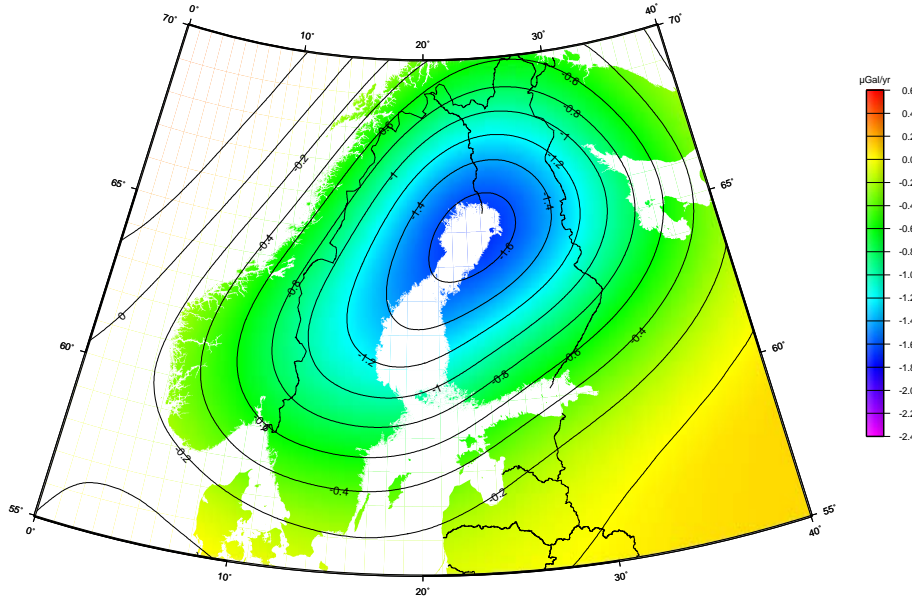Figure 3 shows the LR-model. The direct attraction of the load variations is here not taken into account at all.

Figure 3: LR: $\dot{g}$ computed with a linear relation (-0.154) to predicted $\dot{u}$.

In the BM- and ES-models (Figures 4 and 5) the first term in Green's function for gravity (Eqs 16 and 17) expresses the direct attraction from the surface mass variations. Looking at the present-day $\dot{g}$, only present-day load changes contribute to the direct attraction. In Fennoscandia this means present-day changes in the ocean load (since there is no ice) and these always take place below the point of observation. The BM-model is therefore an inappropriate choice here. Note that in many classical papers, e.g. [20, 13, 30], the Green's function for gravity is expressed in terms of an internal series (with the positive direction of g upwards), which would be the natural choice e.g. for a point located close to (lower than) a large ice mass. It can also be observed in Figures 4 and 5 that the curves are oscillating somewhat, most notably in the North Sea. This effect is due to the Gibb's phenomenon obtained by abruptly truncating the computation of the Green's function (Eq. 16 and 17) at degree 180. The truncation also means that the high frequent nature of the direct attraction from the sea cannot be correctly modelled. The direct from the sea should give a sharp signature along the coastlines (cf. Figure 6) but when it is modelled with a truncated series it propagates incorrectly up on land (Figures 4 and 5).
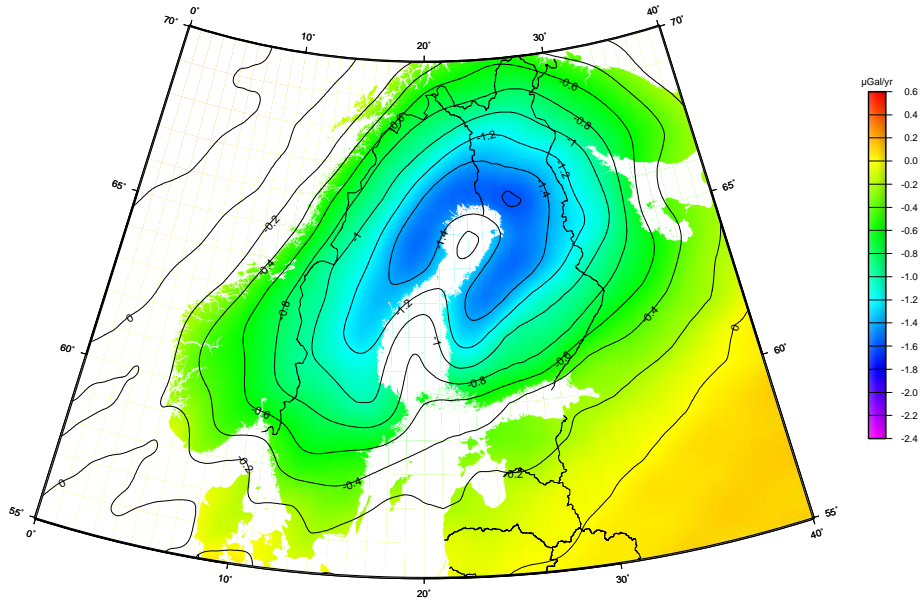
Figure 4: BM - $\dot{g}$ computed with the direct attraction from the load represented in terms of a *internal* series. Max harmonic degree 180.
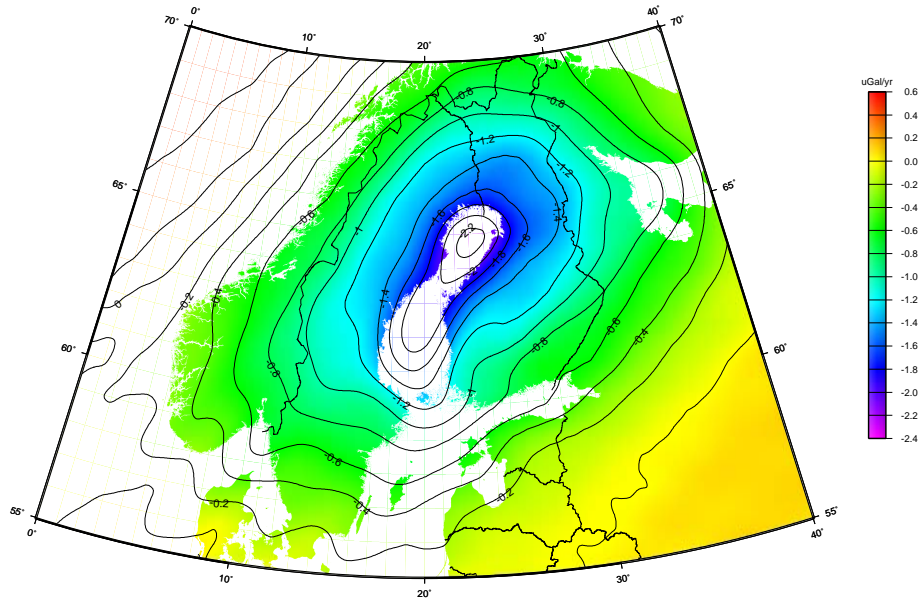

Figure 5: ES - $\dot{g}$ computed with the direct attraction from the load represented in terms of a *external* series. Max harmonic degree 180.

Figure 6 shows the FS-model. The coastline is not plotted separately in this figure but nevertheless exhibits itself in areas where the land uplift (and thereby the change in ocean load) is not close to zero. This is due to the dramatic change of the direct attraction as the coastline is crossed.
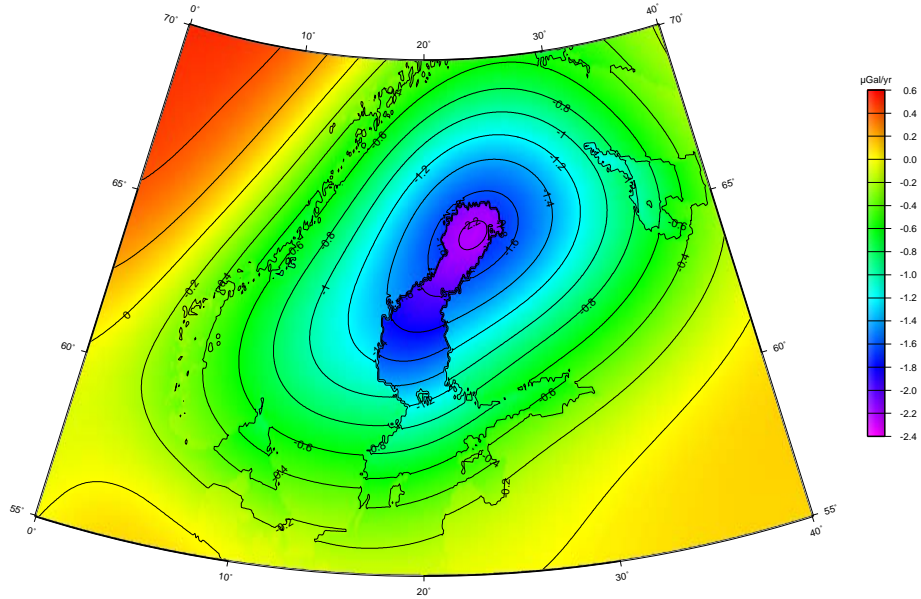
Figure 6: FS - *Full solution* of $\dot{g}$ based on ICE-5G (VM2) and including Generalized Sea Level Equation and a rigorous treatment of the direct attraction.

Solving the Sea Level Equation, (9) and (12), implies convolution in space over the ocean and in time over the full glacial cycle. A number of iterations is required to make the sea surface converge at each time step as well as a number of iterations of the full glacial cycle in order to achieve the final topography (and thereby the coastlines). This makes solving SLE or GLSE a laborious and time consuming work. Its solution is therefore sometimes approximated with a homogenous sea level change over the oceans at each timestep. Figure 7 shows the difference between the FS and this Eustatic Sea Level (ESL) solution. In all other respects these two computations are made in the same way.
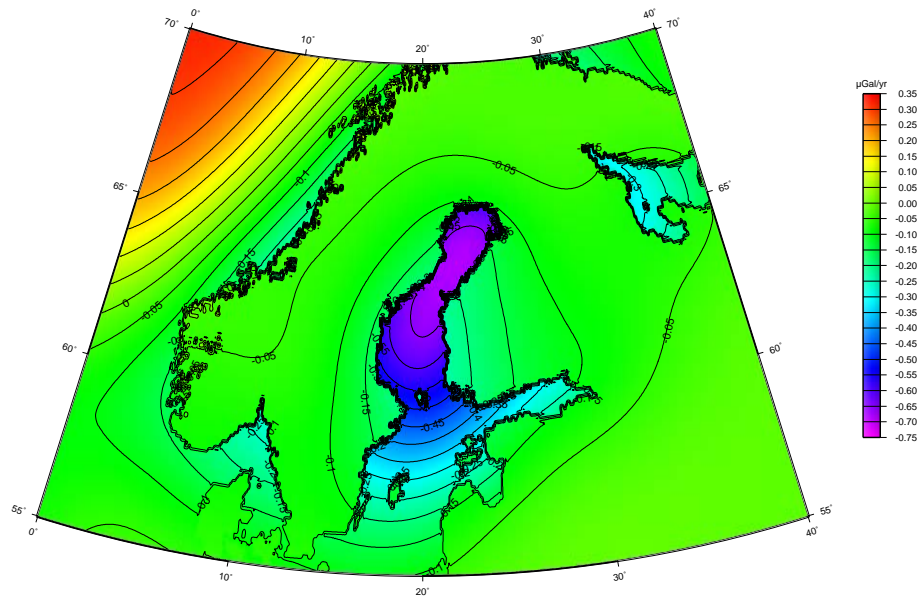
Figure 7: FS-ESL - Full solution of $\dot{g}$ minus solution with eustatic sea level change.

An intermediate step between FS and ESL is to solve Sea Level Equation by not taking into account the migrating shorelines. Figure 8 shows the difference between the FS and the FC (Fixed Coastline) solutions.
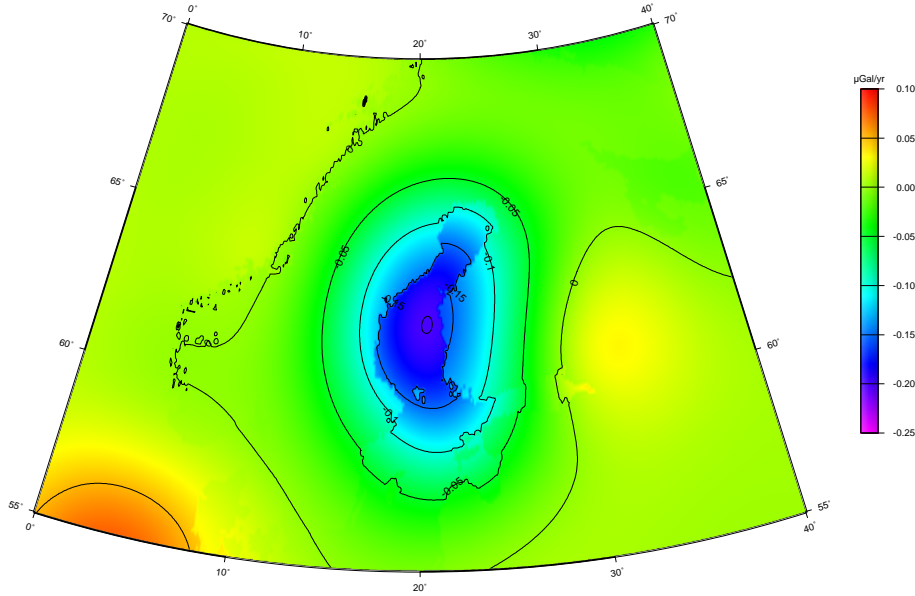
Figure 8: FS-FC - Full solution of $\dot{g}$ minus solution where SLE have been solved with fixed (present) coastline geometry.

5 Discussion of the results

It is already clear that the ES-model is more suitable than the BM-model since, for Fennoscandia, the present-day load variations always take place at lower altitude than the points of observation.

By comparing Figure 5 (ES) and Figure 6 (FS), the effect of the truncation of the direct attraction term in the external Green's function (equation 17) at degree 180 becomes clear. High frequency signals, such as the distinct gravity change along the coastline, are not resolved in ES, in which the distinct signature from FS has smoothened out and the direct effect have propagated to $\dot{g}$-values on land.

In Figure 9 the FS is plotted along a profile at longitude 60.9° in order to illustrate the dramatic change of gravity as the coastline is crossed. To make the plot more general and applicable on an abritrary topography the effect is plotted for three different, constant heights: 1, 10 and 100 meters rather than the true topography. The total $\dot{g}$ signal is dominated by the vertical displacement of the point of observation (uplift = negative $\dot{g}$) and the distinct change as the coastline is crossed is due to the dramatic change in the direct attraction from the sea (relative sea level fall = negative contribution to $\dot{g}$). Note how quickly the direct effect dies out when moving from the coastline into land. In Figure 9 the direct effect is analytically computed using rectangular prisms. This means that the coastline, at this specific location, is perfectly straight, but is otherwise treated

15

in a realistic way, including very high frequencies. In reality the coastline is much more complicated, but the passage from sea to land will look in a similar way.
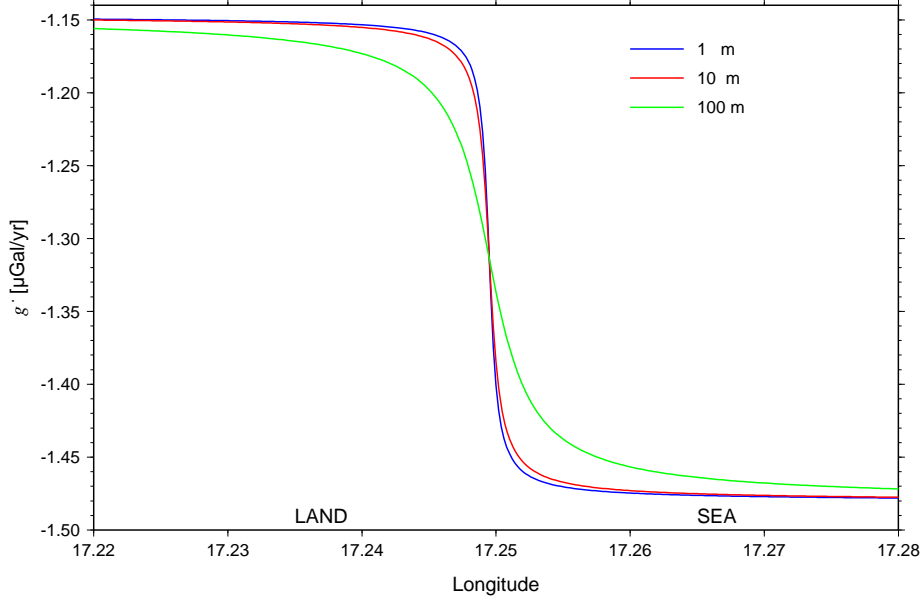

Figure 9: $\dot{g}$ at three different heights (1, 10 and 100 meters above sea level) along a profile at latitude 60.9°. The profile crosses the coastline at longitude 17.25°. The full range of the x-axis in the plot is $\sim$ 3.2 km (0.01° in longitudal direction is $\sim$ 540 m). The relative sea level change $\dot{S}$ in the area is ~ -7.6 mm/yr.

One of the main objectives with this paper is to investigate how good approximation a linear relation between $\dot{g}$ and $\dot{u}$ is, compared to more complex GIA modelling. Let us now compare the full solution of $\dot{g}$ (Figure 6) with the linear model (Figure 3); the difference is illustrated in Figure 10. Since the direct attraction is not considered at all in the linear model, this is the most obvious difference between the two solutions. Over land the difference is less than ± 0.03 μGal/year. Close to the uplift centre, the difference is zero on land, implying that -0.154 is here the best estimate of the ratio $\dot{g}/\dot{u}$. It is also clear from Figure 10 that the LR model is a reasonable approximation, better than BM and ES, at least in non-coastal areas.
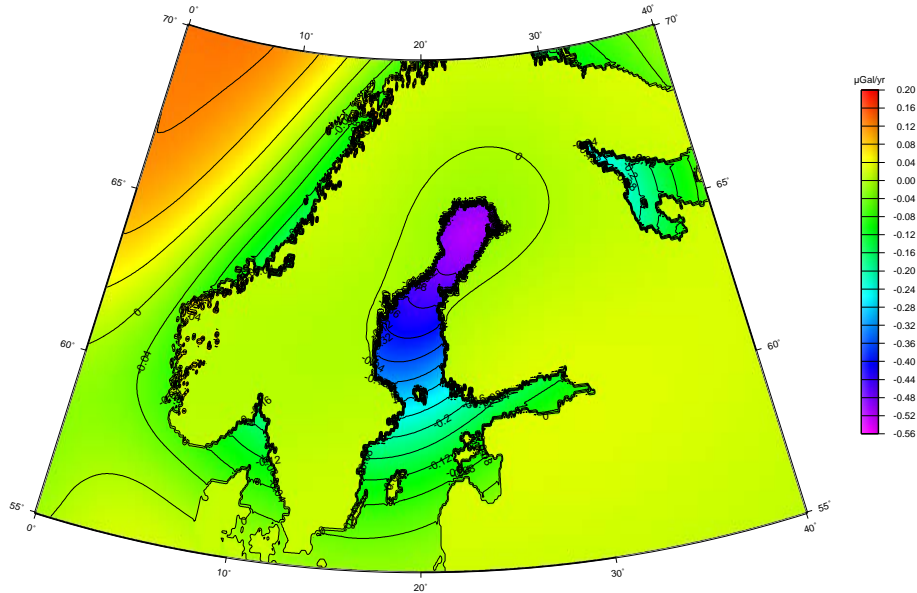
Figure 10: FS-LR: Full solution of $\dot{g}$ (Figure 6) minus the linear model (Figure 3)

.

Figure 11 shows the ratio $\dot{g}/\dot{u}$ for the FS model. Close to the uplift centre this ratio is ~ -0.155 μGal mm^{-1} over land and just exceed -0.20 μGal mm^{-1} over sea, the extra contribution from the direct attraction included. As the land uplift margin is approached the ratio decreases and this trend accelerate as $\dot{g}$ and $\dot{u} \to 0$ (values >-0.10 and <-0.22 μGal mm^{-1} have been blanked with black colour in the figure). An explanation for this can be found in Figure 12 where the predicted $\dot{g}$ and $\dot{u}$ in this region have been plotted against each other. Only points on land have been included ($\sim$ 37000) and from linear regression we have $\dot{g} = -0.1564\dot{u} + 0.024$. The decreasing ratio in Figure 11 is a consequence of the fact that the regression line in Figure 12 does not cross the vertical axis at zero but rather at +0.024, i.e. the gravity rate systematically approaches zero in advance of the uplift rate as one moves away from the uplift maximum. This means that the ratio $\dot{g}/\dot{u}$ first increases, passes through 0 and goes to $+\infty$. Then the ratio changes sign and comes back from $-\infty$.
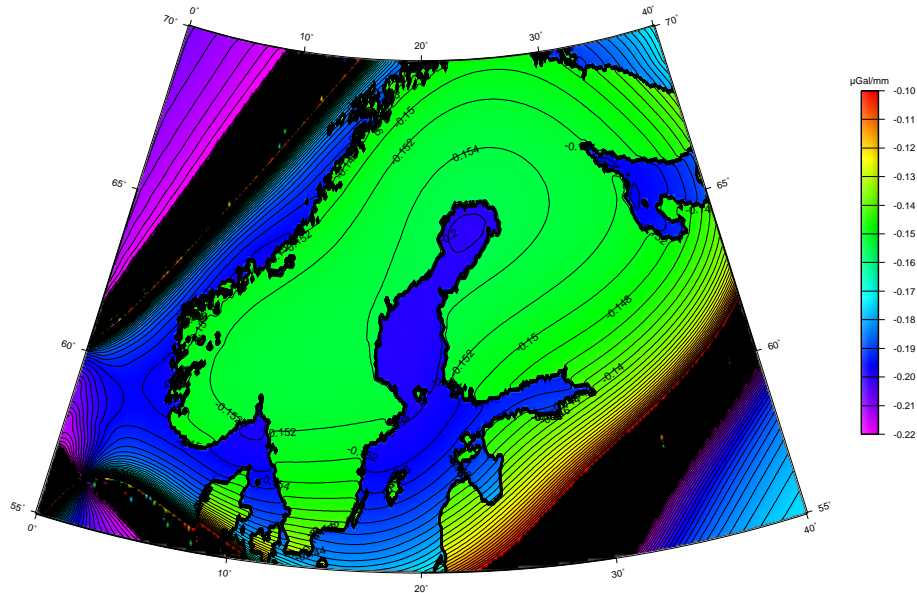
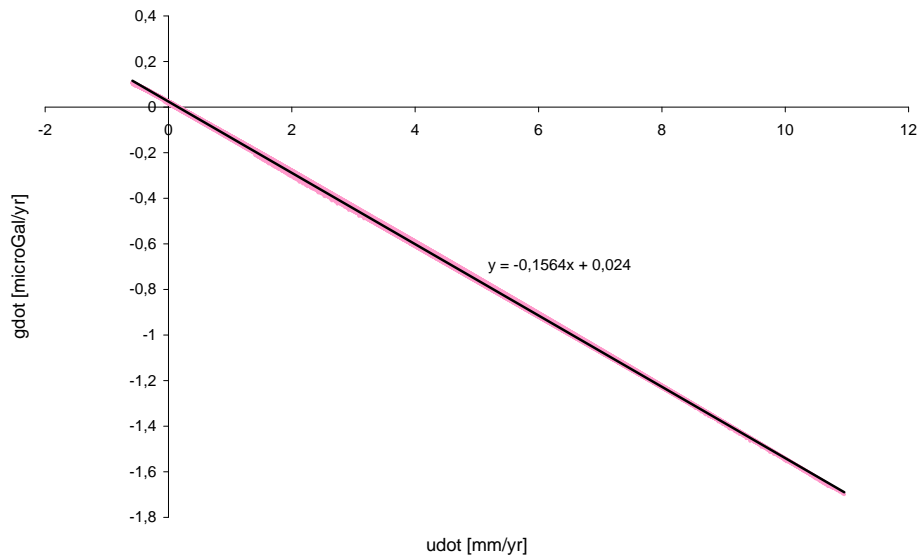Figure 11: Ratio $\dot{g}/\dot{u}$ for the full solution (FS).

Figure 12: Plot of $\dot{g}$ vs. $\dot{u}$ for the full solution (FS). Red dots 37 000 points on evenly distributed over land in Fennoscandia.

The ESL (Figure 7) and FC (Figure 8) model both deviate from the FS model up to 0.25 μGal yr^{-1} over land and more than that, especially for ESL,

over sea.

The results and conclusions above hold for Fennoscandia and the character-istic spatial size and shape of the ice load in this area and might not be true for an ice load of larger or smaller spatial extent. In order to illustrate how displacement and gravity change rates relate to each other in the spectral domain, we consider the example of a unit point load that is applied on the Earth and kept there for 1000 years. We then compute load Love numbers that describe the viscous displacement rate ($\dot{h}_n$) and the viscous gravity change rate

$$\dot{\delta}_n = -2\dot{h}_n + (n+1)\dot{k}_n \tag{23}$$

at 1000 and 5000 years after the deloading event. This is made by convolving the Green's function over the loading in time and by taking the time derivative of the resulting expression; cf. equations (5), (6) and (7). δ_n signifies the bracketed terms in equation (6). The result is presented in Figure 13 and 14. The absolute value of the ratio between $\dot{\delta}_n$ and $\dot{h}_n$ is also plotted, which corresponds to the ratio $\dot{g}/\dot{u}$ in the spectral domain (with opposite sign). It is clearly illustrated that the ratio in question depends on spherical harmonic degree and it follows that, depending upon the dominant degrees in a distributed ice load, the $\dot{g}/\dot{u}$ ratio will be smaller in areas that had a wide ice cover and greater in areas that had a smaller size ice cap.
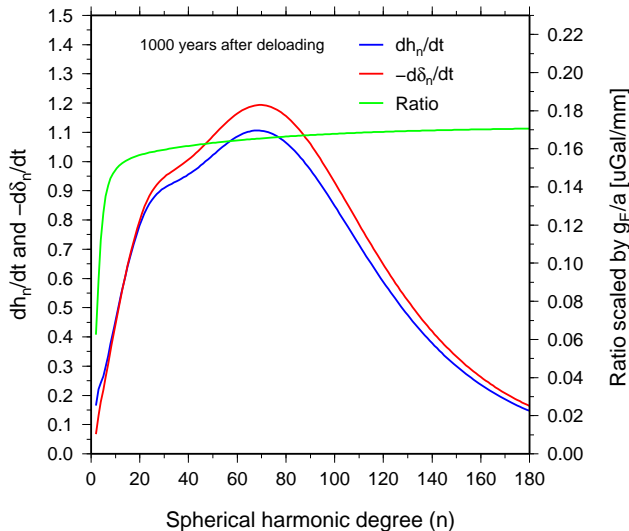

Figure 13: $\dot{h}_n$ and $\dot{\delta}_n$ for a unit point load applied for a time period of 1000 years computed 1000 years after the load has disappeared and the ratio $\dot{\delta}_n/\dot{h}_n$. δ_n signifies the bracketed term in equation (6). Elastic lithosphere 90 km, $\eta_{UM} = 0.52 \cdot 10^{21}$ Pa s, $\eta_{LM} = 2.8 \cdot 10^{21}$ Pa s.

Figure 14: $\dot{h}_n$ and $\dot{\delta}_n$ for a unit point load applied for a time period of 1000 years computed 5000 years after the load has disappeared and the ratio $\dot{\delta}_n/\dot{h}_n$. δ_n signifies the bracketed term in equation (6). Elastic lithosphere 90 km, $\eta_{UM} = 0.52 \cdot 10^{21}$ Pa s, $\eta_{LM} = 2.8 \cdot 10^{21}$ Pa s.
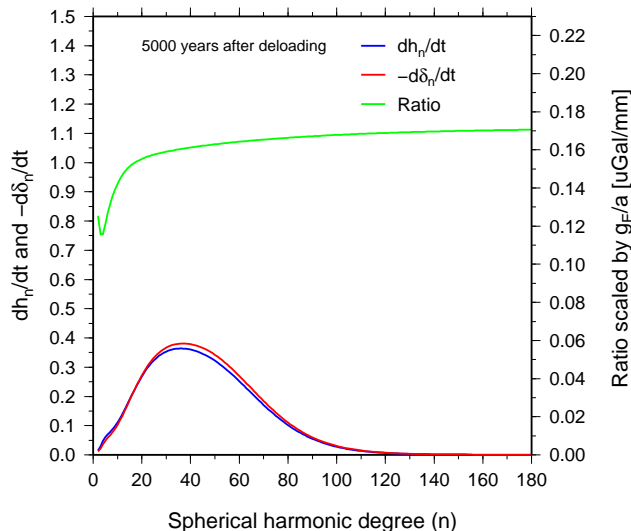
6 Summary and conclusions

In this paper we have discussed different approaches to model the GIA-induced rate of change of surface gravity, $\dot{g}$. A *full GIA-solution* including the Sea Level Equation with time dependent coastline geometry and a rigorous treatment of the direct attraction, have been compared to different simplified models. All modelling has been based on the assumption of a spherical, incompressible, non-rotating, laterally homogenous, viscoelastic Earth and the results have been presented in a series of plots over the Fennoscandian postglacial rebound area.

Within the field of GIA-modelling much effort is put on constraining and evaluating the viscosity profile of the Earth with an increasing amount of geodetic observations of the free air as well as the surface gravity change and the three dimensional deformation of the crust (some recently published results can be found in e.g. [3] and [14], [18], [39]). This has not been the purpose of this work, but rather to investigate different degrees of complexity for the GIA-modelling and show how sensitive $\dot{g}$ predictions in Fennoscandia are to different simplifications.

Since the accuracy of the observed vertical uplift rate, $\dot{u}$, is presently higher compared to the accuracy of the observed gravity change, and since it is much easier to determine $\dot{u}$, the relation between $\dot{u}$ and $\dot{g}$ can be very useful. By comparing the full solution of $\dot{g}$ with a model where $\dot{g}$ is predicted with a linear relation to $\dot{u}$, we can conclude that they agree within ~ 0.02 μGal yr^{-1} in case

we do not take the direct attraction from the secular sea level variations into account.

The direct attraction from the sea reaches several tenths of μGals yr^{-1} over, or very close to, the sea. [29] show that for stations located closer to the sea than $100 \times$ the height of the station, the direct effect can not be neglected; the height effect should be included and a high resolution of the coastline is important. They also show that some stations in the Nordic absolute gravity network [28] are located such that this effect should be treated accurately. We have shown numerically that modelling of the direct attraction by incorporation in the Greens function is not good enough due to the low truncation degree that is typically used (in this paper 180). We also demonstrate significant differences between the Green's functions using an external series or an internal series for the direct effect. Using an internal series adds the contribution from the direct attraction from the sea with the wrong sign. In fact, for Fennoscandia we suggest that it is better to compute $\dot{g}$ from $\dot{u}$ with the fixed-ratio model compared to using the traditional Love number formula for $\dot{g}$ (equation 6) truncated at degree 180. The linear model agrees reasonably well with the full solution of $\dot{g}$. The agreement is better than 0.03 μGal yr^{-1} a few kilometres away from the sea.

We have further compared the full solution with two solutions based on simplified treatment of the ocean. Both simplified models differ from the full solution up to $\sim 0.1 - 0.2$ μGal yr^{-1} over land. Remarkably enough this is almost one order of magnitude larger than the corresponding difference for the linear model but is still smaller than the expected accuray from some 10 years of repeated gravity observations. E.g. [41] reports that from AG-measurements in Belgium, repeated once or twice a year, gravity changes can be resolved with a precision better than 0.37 μGal yr^{-1} after 11 years. It can further be noted that the frequency of re-occupation of the stations in [41] is about twice as high as of the stations in the Nordic AG observational network.

Additionally the ratio $\dot{g}/\dot{u}$ has been studied for Fennoscandia. Due to the fact that $\dot{g}$ moves to zero and changes sign before $\dot{u}$, when one moves away from the land uplift maximum, the negative ratio first increases, then changes sign and finally goes to infinity. However, both $\dot{g}$ and $\dot{u}$ are small when this happens, which implies that the $\dot{g}$ value that is obtained by using the ratio -0.154 μGal mm^{-1} is acceptable with respect to measurement uncertainty.

The results in this paper should be seen as a contribution to the understanding of how sensitive $\dot{g}$ in Fennoscandia is to different parts of the GIA-modelling. In future work we will incorporate and compare the effects from the first degree load Love numbers, rotational feedback and compressibility in the earth models. Based on the comprehensive work carried out in this region, geodetic observations as well as geophysical modelling (c.f. [40]), we foresee successively improved ice models, three dimensional Earth models and predictions of $\dot{g}$.

7 Acknowledgement

References

[1] J. Ågren. *Regional Geoid Determiniation Methods for the Era of Satellite Gravimetry. Numerical Investigations Using Synthetic Earth Gravity Models.* PhD thesis, Royal Institute of Technology, Stockholm, Sweden, 2004.

[2] J. Ågren and R. Svensson. Postglacial land uplift model and system definition for the new Swedish height system RH 2000. LMV-Rapport 2007:4, Lantmäteriet, the Swedish mapping, cadastral and land registration authority, 2007.

[3] D.F. Argus and W.R. Peltier. Constraining models of postglacial rebound using space geodesy: A detailed assessment of model ICE-5G (VM2) and its relatives. *Geophys. J. Int.*, 181:697–723, 2010.

[4] B.G. Bills and T.S. James. Late Quaternary variations in relative sea level due to glacial cycle polar wander. *Geophys. Res. Lett.*, 23:3023–3026, 1996.

[5] L.M. Cathles. *The viscosity of the Earth's mantle.* Princeton University Press, 1975.

[6] C. de Linage, J. Hinderer, and Y. Rogister. A search for the ratio between gravity variation and vertical displacement due to a surface load. *Geophysical Journal International*, 171:986–994, 2007.

[7] A.M. Dziewonski and D.L. Anderson. Preliminary reference earth model. *Physics of the Earth and Planetary Interiors*, 25:297–356, 1981.

[8] M. Ekman. A consistent map of the postglacial uplift of Fennoscandia. *Terra Nova*, 8:158–165, 1996.

[9] M. Ekman. *The changing level of the Baltic Sea during 300 years: A clue to understanding the Earth.* Summer Institute for Historical Geophysics, 2009.

[10] M. Ekman and J. Mäkinen. Resent postglacial rebound, gravity change and mantle flow in Fennoscandia. *Geophysical Journal International*, 126:229–234, 1996.

[11] M. Fang and B.H. Hager. Vertical deformation and absolute gravity. *Geophysical Journal International*, 146(2):539–548, 2001.

[12] W.E. Farrel and J.A. Clark. On postglacial sea level. *Geophys. J. R. astr. Soc.*, 46:467–667, 1976.

[13] W.E. Farrell. Deformation of the Earth by surface loads. *Reviews of Geophysics and Space Physics*, 10(3):761–797, 1972.

[14] E.M. Hill, J.L. Davis, M.E. Tamisiea, and M. Lidberg. Combination of geodetic observations and models for glacial isostatic adjustment fields in Fennoscandia. *Journal of Geophysical Research*, 115(B07403), 2004.

[15] P. Johnston. The effect of spatial non-uniform water loads on predictions of sea level change. *Geophys. J. Int.*, 114115:615–634, 1993.

[16] R.A. Kendall, J.X. Mitrovica, and G.A. Milne. On post-glacial sea level -II. Numerical formulation and comparative results on spherically symmetric models. *Geophys. J. Int.*, 161:679–706, 2005.

[17] K. Lambeck, C. Smither, and P. Johnston. Sea-level change, glacial rebound and mantle viscosity for northern Europe. *Geophys. J. Int.*, 134:102–144, 1998.

[18] M. Lidberg, J.M. Johansson, H.-G. Scherneck, and G.A. Milne. Recent results based on continuous GPS observations of the GIA process in Fennoscandia from BIFROST. *Journal of Geodynamics*, 50:8–18, 2010.

[19] I.M. Longman. A Green's function for determining the deformation of the Earth under surface mass loads. 1. Theory. *Journal of Geophysical Research*, 67(2):845–850, 1962.

[20] I.M. Longman. A Green's function for determining the deformation of the Earth under surface mass loads. 2. Computations and numerical results. *Journal of Geophysical Research*, 68:485–496, 1963.

[21] J. Mäkinen, M. Ekman, Å. Midtsundstad, and O. Remmer. The Fennoscandian land uplift gravity lines 1966-1984. Rep. Finn. Geod. Inst. 85:4, Finnish Geodetic Institute, 1986.

[22] J. Mäkinen, A. Engfeldt, B.G. Harsson, H. Ruotsalainen, G. Stykowski, T. Oja, and D. Wolf. The Fennoscandian land uplift gravity lines 1966-2004. In Christopher Jekeli, Luisa Bastos, and Joana Fernandes, editors, *Gravity, Geoid and Space Missions*, volume 129 of *International Association of Geodesy Symposia*, pages 328–332. Springer Berlin Heidelberg, 2005.

[23] S. Mazotti, A. Lambert, J. Henton, T.S. James, and N. Courtier. Absolute gravity calibration of GPS velocities and glacial isostatic adjustment in mid-continent North America. *Geophys. Res. Lett.*, 38(L24311), 2011.

[24] G.A. Milne, J.X. Mitrovica, H.-G. Scherneck, J.L. Davis, J.M. Johansson, H. Koivula, and M. Vermeer. Continuous GPS measurements of postglacial adjustment in Fennoscandia: 2. Modeling results. *Journal of Geophysical Research*, 109(B02412), 2004.

[25] J.X. Mitrovica and G.A. Milne. On post-glacial sea level: I. General theory. *Geophys. J. Int.*, 154:253–267, 2003.

[26] D. Nagy, G. Papp, and J. Benedek. The gravitational potential and its derivatives for the prism. *Journal of Geodesy*, 74:552–560, 2000.

[27] National Oceanic and Atmospheric Administration (NOAA). ETOPO1 global relief model. `http://www.ngdc.noaa.gov/mgg/global/global.html`. from National Geophysical Data Center home page; accessed 09-April-2011.

[28] P.-A. Olsson. Contribution to the modelling of postglacial gravity change in Fennoscandia. Licentiate thesis, Chalmers University of Technology, Gothenburg, 2011.

[29] P.-A. Olsson, H.-G. Scherneck, and J. Ågren. Effects on gravity from non-tidal sea level variations in the Baltic Sea. *Journal of Geodynamics*, 48:151–156, 2009.

[30] W.R. Peltier. The impulse response of a Maxwell Earth. *Reviews of Geophysics and Space Physics*, 12(4):649–669, 1974.

[31] W.R. Peltier. Glacial-isostatic adjustment - II. The inverse problem. *Geophysical Journal of the Royal Astronomical Society*, 46:669–705, 1976.

[32] W.R. Peltier. Global glacial isostasy and the surface of the ice-age Earth: The ICE-5G (VM2) model and GRACE. *Annu. Rev. Earth. Planet. Sci.*, 32:111–149, 2004.

[33] W.R. Peltier. Submissions of post-glacial rebound predictions by Peltier. `http://www.sbl.statkart.no/projects/pgs/authors/peltier/`, 2004. from home page for Special Bureau for Loading; accessed 28-March-2011.

[34] W.R. Peltier and J.T. Andrews. Glacial-isostatic adjustment - I. The forward problem. *Geophysical Journal of the Royal Astronomical Society*, 46(3):605–646, 1976.

[35] H.-G. Scherneck, J.M. Johansson, G. Elgered, J.L. Davis, B. Jonsson, G. Hedling, H. Koivula, M. Ollikainen, M. Poutanen, M. Vermeer, J.X. Mitrovica, and G.A. Milne. BIFROST: Observing the three-dimensional deformation of Fennoscandia. In J.X. Mitrovica and B.L.A. Vermeersen, editors, *Ice Sheets, Sea Level and the Dynamic Earth*, Geodynamic Series 29, pages 69–93. American Geophysical Union, 2002.

[36] G. Spada. *Solving the sea level equation, part I, Theory*. Samizdat Press, Golden, White River Junction, USA, 2003.

[37] G. Spada. *TABOO User Guide*. Samizdat Press, Golden, White River Junction, USA, 2003.

[38] G. Spada. *The theory behind TABOO - a posT glAcial reBOund calculatOr*. Samizdat Press, Golden, White River Junction, USA, 2003.

[39] H. Steffen and P. Wu. Glacial isostatic adjustment in Fennoscandia - A review of data and modeling. *Geophys. J. Int.*, 182:1295–1310, 2010.

[40] H. Steffen, P. Wu, and H. Wang. Determination of the Earth's structure in Fennoscandia from GRACE and implications for the optimal post-processing of GRACE data. *Journal of Geodynamics*, 52:169–204, 2011.

[41] M. Van Camp, O. de Viron, H.G. Scherneck, K.G. Hinzen, S.D.P. Williams, T. Lecocq, Y. Quinif, and T. Camelbeeck. Repeated absolute gravity measurements for monitoring slow intraplate vertical deformation in western Europe. *Journal of Geophysical Research*, 116(B08402), 2011.

[42] J. Wahr, H. DaZhong, and A. Trupin. Predictions of vertical uplift caused by changing polar ice volumes on a viscoelastic earth. *Geophys. Res. Lett.*, 22(8):977–980, 1995.

[43] P. Wu. Response of a Maxwell Earth to applied surface mass loads:Glacial Isostatic Adjustment. Master's thesis, Department of Physics, University of Toronto, 1978.

[44] P. Wu and W.R. Peltier. Viscous gravitational relaxation. *Geophys. J. R. astr. Soc.*, 70:435–485, 1982.

[45] P. Wu and W.R. Peltier. Glacial isostatic adjustment and the free air gravity anomaly as a constraint on deep mantle viscosity. *Geophys. J. R. astr. Soc.*, 74:377–449, 1983.